Determinants of Potency on α-Conotoxin MII, a Peptide Antagonist of Neuronal Nicotinic Receptors†

Drew Everhart,‡ G. Edward Cartier,§,|| Arun Malhotra,⊥ Aldrin V. Gomes,‡ J. Michael McIntosh,§,# and Charles W. Luetje*,‡

Departments of Molecular and Cellular Pharmacology and Biochemistry and Molecular Biology, University of Miami School of Medicine, P.O. Box 016189, Miami, Florida 33101, and Departments of Biology and Psychiatry, University of Utah, Salt Lake City, Utah 84112

Received December 4, 2003

ABSTRACT: α-Conotoxin MII, a peptide toxin isolated from *Conus magus*, antagonizes a subset of neuronal nicotinic receptors. Rat α3β2 receptors, expressed in *Xenopus* oocytes, are blocked with an IC_{50} of 3.7 ± 0.3 nM. To identify structural features that determine toxin potency, a series of alanine-substituted toxins were synthesized and tested for the ability to block the function of α3β2 receptors. Circular dichroism and protein modeling were used to assess the structural integrity of the mutant toxins. Three residues were identified as major determinants of toxin potency. Replacement of asparagine 5, proline 6, or histidine 12 with alanine resulted in >2700-fold, 700-fold, and ~2700-fold losses in toxin potency, respectively. A decrease in pH improved toxin potency, while an increase in pH eliminated toxin blockade, suggesting that, in the active form of the toxin, histidine 12 is charged. The imidazole ring of histidine 12 protrudes from one side, while asparagine 5 and proline 6 are located at the opposite end of the toxin structure. The side chains of these three residues are exposed on the surface of the toxin, suggesting that they directly interact with the α3β2 receptor.

Nicotinic acetylcholine receptors (nAChRs)[1] are expressed throughout the nervous system and belong to a family of ligand-gated ion channels that includes receptors for GABA, glycine, and serotonin (*1*). Neuronal nAChRs are assembled from a family of at least 12 subunits: α2−10 and β2−4 (*2*). When expressed in *Xenopus* oocytes, a variety of functional subunit combinations possessing unique pharmacological properties can be formed. These pharmacological differences have been exploited to reveal structural and functional details of neuronal nicotinic receptors (*2*).

α-Conotoxins are small, disulfide-rich peptide neurotoxins derived from the venom of the *Conus* genus of predatory marine snails. They competitively inhibit muscle and neuronal nicotinic nAChRs to varying degrees (*3*). All α-conotoxins have a conformationally constrained two-loop structure formed by two disulfide bridges. However, they differ in the number and type of residues in each loop. These differences in loop characteristics and residue composition form the basis for each toxin's receptor subtype specificity (*3*).

α-Conotoxin MII (MII) is a 16 amino acid peptide (GCCSNPVCHLEHSNLC) isolated from the venom of *Conus magus*. MII toxin and α-conotoxin PnIA (PnIA) from *Conus pennaceus* selectively antagonize a subset of neuronal nicotinic receptors including α3β2 and several α6-containing receptors (*4*−*9*). The ability of both MII and PnIA to antagonize α3β2 receptors is interesting, because while both toxins have the same disulfide-bonding pattern (C2−C8, C3−C16), they differ at 9 of the 12 noncysteine residues and they interact with overlapping, but distinct groups of amino acid residues on the receptor. On the α3 subunit, we have previously identified K185 and I188 as determinants of MII sensitivity and P182, I188, and Q198 as determinants of PnIA sensitivity (*9*, *10*).

Here we use alanine-scanning mutagenesis to identify residues on the MII toxin that determine potency at α3β2 neuronal nAChRs. Each non-cysteine residue on MII was replaced with alanine, and the IC_{50} for antagonism of α3β2 receptors was determined. Cysteine residues could not be examined by this approach, due to their critical role in the structure of the toxin. Circular dichroism (CD) and protein modeling were used to confirm the structural integrity of each mutant toxin. Using this approach, we have identified three determinants of potency on α-conotoxin MII.

EXPERIMENTAL PROCEDURES

Materials. Xenopus laevis frogs were purchased from Nasco (Fort Atkinson, WI). The care and use of *X. laevis*

† Supported by NIH Grant DA08102 (C.W.L.), NIH Grant MH53631 (J.M.M.), Florida Biomedical Research Foundation Grant BM030 (A.M.), and American Heart Association Florida/Puerto Rico Affiliate SDG-0130456B (A.M.).

* Corresponding author. Tel: (305) 243-4458. Fax: (305) 243-4555. E-mail: cluetje@chroma.med.miami.edu.

‡ Department of Molecular and Cellular Pharmacology, University of Miami School of Medicine.

§ Department of Biology, University of Utah.

|| Present address: Cognetix, Inc., 421 Wakara Way, Suite 201, Salt Lake City, UT 84108.

⊥ Department of Biochemistry and Molecular Biology, University of Miami School of Medicine.

Department of Psychiatry, University of Utah.

[1] Abbreviations: MII, α-conotoxin MII; nAChRs, nicotinic acetylcholine receptors; PnIA, α-conotoxin PnIA; RMSD, root-mean-square deviation.

10.1021/bi036180h CCC: $27.50
Published on Web 02/18/2004

frogs in this study were approved by the University of Miami Animal Research Committee and meet the guidelines of the National Institutes of Health. RNA transcription kits were from Ambion (Austin, TX). Collagenase B was from Boehringer-Mannheim (Indianapolis, IN). All other reagents were from Sigma (St. Louis, MO). Wild-type and mutant MII toxins were synthesized, proper disulfide bond formation was achieved, and the toxins were purified as previously described (*4*, *6*).

Expression of Neuronal nAChRs in X. laevis Oocytes. cDNA clones encoding rat α3 and β2 subunits were used as templates for generating $m^7G(5')ppp(5')G$-capped cRNA using in vitro cRNA synthesis kits from Ambion (Austin, TX). Mature *X. laevis* frogs were anesthetized by submersion in 0.1% 3-aminobenzoic acid ethyl ester, and oocytes were surgically removed. Follicle cells were removed by treatment with collagenase B for 2 h at room temperature. Stage V oocytes were individually injected with 3−10 ng of each subunit cRNA in 50 nL of water and incubated at 18 °C in Barth's saline (88 mM NaCl, 1 mM KCl, 2.4 mM $NaHCO_3$, 0.3 mM $CaNO_3$, 0.41 mM $CaCl_2$, 0.82 mM $MgSO_4$, 100 μg/mL gentamicin, 15 mM HEPES, pH 7.6) for 2−7 days.

Electrophysiological Methods. Current responses were measured under a two-electrode voltage clamp, at a holding potential of −70 mV, using an OC-725C voltage clamp unit (Warner Instruments, Hamden, CT). Micropipets were filled with 3 M KCl and had resistances of 0.3−2.0 MΩ. Current responses were captured, stored, and analyzed on a Macintosh G3 computer using AxoGraph 4.6 software (Axon Instruments, Union City, CA). Oocytes were perfused at room temperature (20−25 °C), in a chamber constructed from $^1/_8$ in. inner diameter Tygon tubing, with perfusion solution (115 mM NaCl, 1.8 mM $CaCl_2$, 2.5 mM KCl, 0.1 μM atropine, 10 mM HEPES, pH 7.2). Perfusion was continuous (except during toxin incubations) at a rate of ∼2 mL/min. ACh was applied diluted in perfusion solution. Toxin was applied diluted in perfusion solution supplemented with 100 μg/mL BSA. In Figures 1 and 2 and Table 1, the extent of receptor blockade was determined by comparing the ACh-induced peak current response following a 5 min incubation with toxin, to the average of three ACh-induced peak current responses preceding the toxin incubation. The ACh concentration used in all experiments was 70 μM, the EC_{50} for α3β2 neuronal nicotinic receptors (*11*). During the postincubation ACh application, the appropriate concentration of toxin was included. However, BSA was not included because previous experiments showed modest (23 ± 9%, $n = 3$), rapidly reversible (<1 s) inhibition of α3β2 receptors by BSA (100 μg/mL) (*9*). For the pH sensitivity experiment, three preincubation ACh responses were first obtained at pH 7.2. MII toxin (supplemented with BSA) was then applied for 5 min at various pH values (5.5, 7.2, and 8.9). Oocytes were then rinsed back into normal perfusion solution (pH 7.2) for 15 s, followed by application of ACh (at pH 7.2). In the absence of toxin, 5 min incubation at pH 5.5 or 8.9 had no effect on ACh response amplitude (data not shown).

Data Analysis. Data were fit using PRISM 3 software (GraphPad, San Diego, CA). MII dose-inhibition data were fit using the equation $I = I_{max}/[1 + (X/IC_{50})^n]$, where I is the current response in the presence of antagonist concentration X, I_{max} is the maximum current, IC_{50} is the antagonist concentration producing the half-maximal inhibition, and n is the Hill coefficient. IC_{50} values derived from Figure 2 were used to calculate differences in toxin potency.

Far-UV Circular Dichroism Analysis. CD spectra of 20 μM solutions of wild-type and mutant MII toxin preparations were recorded on a Jasco J-720 spectropolarimeter with a cell path length of 0.1 cm at room temperature in 10 mM Tris and 60 mM NaCl, pH 7.0. Scans were acquired from 190 to 250 nm, with a bandwidth of 1 nm, a speed of 50 nm/min, and a resolution of 0.2 nm. A total of 10 scans/sample were averaged, and baselines were subtracted. Four samples of each toxin were analyzed. Analysis and processing of data were carried out with the Jasco system software (Windows standard analysis, version 1.20). Mean residue ellipticity (θ_{MRE}, in deg·cm^2·dmol^{-1}) for each spectrum was calculated from the formula $\theta_{MRE} = \theta/(10Crl)$, where θ is the measured ellipticity in millidegrees, Cr is the mean residue molar concentration, and l is the path length in centimeters. The α-helical content was calculated from the experimentally determined formula $\theta = -30300f_H - 2340$, where f_H is the fraction of α-helical content ($f_H \times 100$, expressed as a percentage) at 222 nm (*12*).

Generation of Homology Models. Three-dimensional models were constructed using the program MODELLER 6 (*13*) on a Silicon Graphics Indigo2 Extreme workstation using the script "model". Disulfide bonds in the toxin template structure were explicitly included during homology model refinement. Each mutant toxin was modeled using the coordinates for the NMR-derived structure of wild-type α-conotoxin MII as template (*14*) (PDB ID 1M2C, model 1). Ten models for each mutant toxin were produced with energy refinement handled within the program. Models were inspected visually and with PROCHECK (*15*) for inappropriate stereochemistry (clashing side chains, disallowed torsion angles, etc.). The images in Figure 3 were produced using RIBBONS (*16*). The positions of α carbons in the mutant toxin models were compared to the wild-type toxin structure using LSQMAN (*17*) to obtain Cα RMSD values. To display electrostatic surfaces, protons were added to the wild-type and mutant toxin structures using the PROTEUS program distributed as part of the GRASP 1.2.5 package (*18*). Histidines were assigned an overall charge of +1 on the basis of the results of the pH dependence experiments. Electrostatic surfaces were then calculated with GRASP 1.2.5 (*18*) using the parse3.crg partial charge set. Images in Figure 5 were produced using GRASP.

RESULTS

α-CTx-MII antagonizes α3β2 neuronal nicotinic receptors. A 5 min incubation with 10 nM MII inhibited the subsequent current response to 70 μM ACh by 76% (Figure 1A). Some alanine mutations, such as N14A, had little or no effect on the potency of the MII toxin. Similar to wild-type MII, incubation with 10 nM N14A resulted in 73% receptor inhibition (Figure 1B). In contrast, some mutations, such as H12A, had large effects on toxin potency. In Figure 1C, we show that 10 μM H12A is required to achieve 51% receptor inhibition.

To compare the effect of each of the 12 mutations, we measured receptor blockade by a range of toxin concentrations and obtained IC_{50} values (Figure 2 and Table 1). Wild-type α-CTx-MII antagonized α3β2 receptors with an IC_{50}

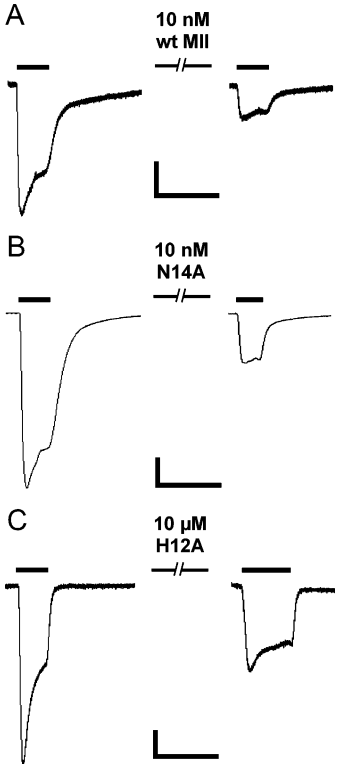

FIGURE 1: Variable effects of mutations on α-conotoxin MII potency. Current responses of *Xenopus* oocytes expressing α3β2 neuronal nicotinic receptors to 70 μM ACh before and after 5 min incubation with (A) 10 nM α-conotoxin MII (scale: 50 nA, 20 s), (B) 10 nM N14A mutant (scale: 200 nA, 20 s), or (C) 10 μM H12A mutant (scale: 50 nA, 20 s).

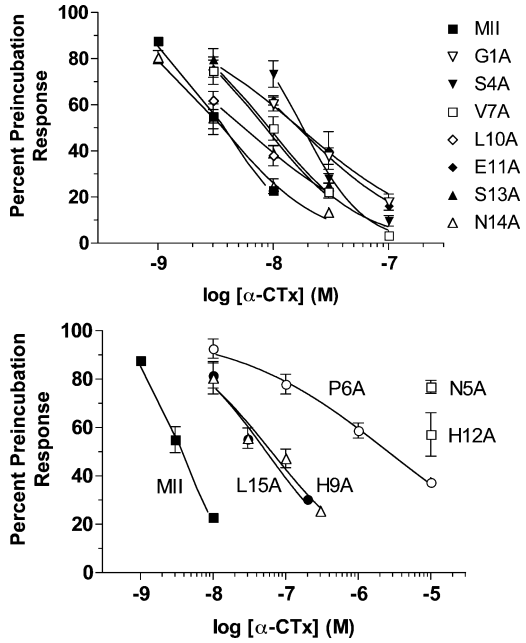

FIGURE 2: Inhibition of α3β2 neuronal nicotinic receptors by wild-type and mutant MII toxins. The response to 70 μM ACh after 5 min incubation with various concentrations of wild-type and mutant MII toxin is presented as a percentage of the preincubation ACh response. Each point is the mean ± SEM of three to five oocytes. Data were fit as described in Experimental Procedures.

of 3.7 ± 0.3 nM. None of the alanine mutations increased toxin potency. Mutations that had little or no effect (defined as a change in the IC_{50} of less than 3-fold) included V7A, L10A, S13A, and N14A. Several mutations (G1A, S4A, and E11A) had modest effects on potency (a loss of 3−5-fold). Two mutations (H9A and L15A) had moderate effects on potency (17- and 15-fold, respectively). Three mutations had substantial effects on toxin potency. The P6A toxin mutant inhibited α3β2 receptors with an IC_{50} of 2.6 μM, a 700-fold loss of potency. The N5A mutation resulted in a >2700-fold loss of potency, with 10 μM toxin inhibiting receptor function by 23%. The H12A mutation resulted in an ∼2700-fold loss of potency, with 10 μM toxin inhibiting receptor function by 43%.

Table 1: Potency of Wild-Type and Mutant α-Ctx-MII[a]

toxin	IC_{50} (nM)	n_H	fold change
MII	3.7 ± 0.3	1.3 ± 0.1	
G1A	16.5 ± 1.8	0.8 ± 0.1	4.5
S4A	18.1 ± 1.8	1.7 ± 0.3	4.9
N5A	>10000		>2700
P6A	2590 ± 553	0.4 ± 0.1	700
V7A	9.2 ± 1.0	1.1 ± 0.1	2.5
H9A	63.8 ± 11.1	0.6 ± 0.1	17
L10A	5.6 ± 0.8	0.8 ± 0.1	1.5
E11A	16.9 ± 2.9	0.7 ± 0.1	4.6
H12A	∼10000		∼2700
S13A	8.6 ± 1.0	1.1 ± 0.2	2.3
N14A	3.6 ± 0.5	1.0 ± 0.2	1.0
L15A	54.3 ± 8.6	0.7 ± 0.1	15

[a] IC_{50} and n_H values were derived from Figure 2 as described in Experimental Procedures.

The losses in potency observed with the N5A, P6A, H9A, H12A, and L15A mutations suggest that the residues at these positions are important participants in the interaction between the toxin and the receptor. However, it is also possible that these changes in potency are due to the mutations being poorly tolerated by the toxin structure. The NMR-derived structure shown in Figure 3A contains some α-helical content, suggesting that CD would be useful in assessing the structural integrity of the toxins. CD analysis on our wild-type MII preparation indicated 31% α-helical content (Table 2), consistent with the structure in Figure 3A, in which 5 of 16 residues form one α-helical turn. CD analysis indicated that all of the mutant toxin preparations possessed some α-helical content, suggesting that none of the toxins were completely unfolded. Some of the mutant toxins had α-helical content similar to that of wild-type MII. For example, the H12A mutant, which was ∼2700-fold less potent than wild-type toxin (Table 1), had a similar α-helical content (Table 2). This suggests that it is the loss of the histidine side chain, rather than a change in the overall toxin structure, that is responsible for the loss in potency. The other two mutants displaying large losses in potency, N5A and P6A, had somewhat lower helical content than the wild-type toxin (22% and 23%, respectively), perhaps reflecting the location of these positions at the start of the α-helix (with only 16 amino acids in the peptide, each residue in the helix contributes a helical content of 6%). Some mutants displayed a substantially greater or lesser α-helical content than the wild-type preparation. The H9A and L15A mutants, each displaying a moderate loss of potency, had twice and half the helical content of wild-type toxin, respectively. This suggests that, for these mutations, changes in overall toxin structure may, at least in part, be responsible for the loss of potency.

We also assessed the structural integrity of the mutant toxins by generating homology models, using the NMR-

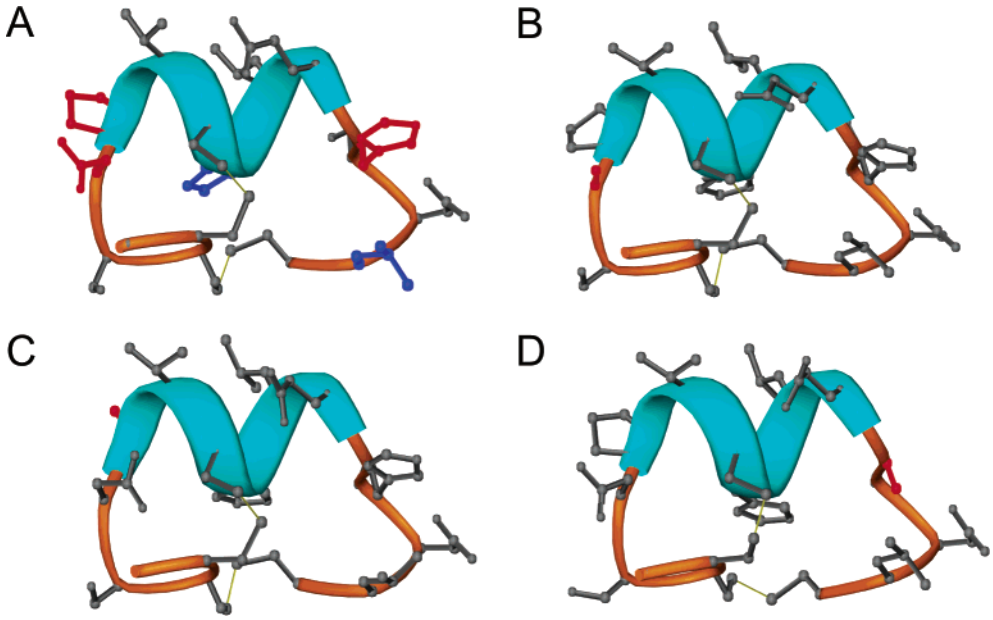

FIGURE 3: Structures of wild-type and mutant MII toxins. (A) The lowest energy NMR structure from Shon et al. (*14*) is shown. The N5, P6, and H12 residue side chains are shown in red. H9 and L15 are in blue. The C2−C8 and C3−C16 disulfide bonds are in yellow. (B) The modeled structure of the N5A mutant is shown with A5 in red. (C) The modeled structure of the P6A mutant is shown with A6 in red. (D) The modeled structure of the H12A mutant is shown with A12 in red. Images were generated using RIBBONS (*16*).

Table 2: Structural Integrity of Wild-Type and Mutant α-Ctx-MII[a]

toxin	α-helical content (%)	α-carbon RMSD (Å)
α-Ctx-MII	31.2 ± 0.5	0.96 ± 0.10
G1A	39.8 ± 0.7	0.50 ± 0.05
S4A	49.4 ± 2.9	0.56 ± 0.07
N5A	21.7 ± 1.9	0.49 ± 0.05
P6A	23.4 ± 1.3	0.46 ± 0.04
V7A	42.3 ± 1.2	0.48 ± 0.03
H9A	68.9 ± 0.7	0.48 ± 0.04
L10A	64.6 ± 1.1	0.52 ± 0.03
E11A	44.9 ± 1.3	0.50 ± 0.04
H12A	28.3 ± 1.0	0.61 ± 0.05
S13A	51.0 ± 5.4	0.59 ± 0.07
N14A	42.5 ± 2.9	0.65 ± 0.07
L15A	16.1 ± 1.6	0.54 ± 0.04

[a] The α-helical content of the wild-type and mutant toxin preparations was determined using circular dichroism, as described in Experimental Procedures. The α-carbon RMSD values for each mutant toxin model were calculated as described in Experimental Procedures. The α-carbon RMSD value for the wild-type toxin was calculated by comparing the 14 lowest energy NMR structures in Shon et al. (*14*).

derived MII structure as a template. All of the mutant toxins modeled well, yielding structures that looked very similar to the wild-type structure. This is not surprising because most of the side chains face outward into solution, allowing substitutions to be tolerated. Structures for the N5A, P6A, and H12A mutants are shown in Figure 3. To obtain a more quantitative measure of the similarity of the mutant structures to the wild-type structure, we calculated the α carbon rmsd values for the 10 preliminary models that were generated for each mutant (see Experimental Procedures). The variation of the model structures from the wild-type structure was less than the variation observed among the NMR-derived wild-type structures (Table 2).

Mutation of either of the histidine residues in MII resulted in a loss of toxin potency, with the H12A mutation having a particularly dramatic effect. To determine whether it is the protonated imidazolium or the neutral imidazole form of

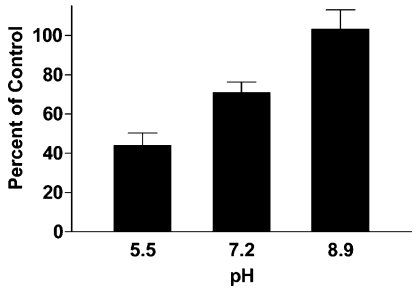

FIGURE 4: MII toxin potency is pH dependent. The response to 70 μM ACh after 5 min incubation with 3 nM MII toxin at various pH values is presented as a percentage of the preincubation ACh response (mean ± SEM, $n = 3$).

histidine that is involved in the toxin−receptor interaction, we measured the extent of receptor blockade achieved by incubation with 3 nM MII toxin at different pH values (Figure 4). Responses to 70 μM ACh in our standard perfusion solution (pH 7.2) were measured before and after a 5 min incubation with toxin at pH 5.5, 7.2, or 8.9 (see Experimental Procedures). At a pH of 5.5, MII toxin was more potent, with 3 nM toxin inhibiting receptor function by 56.1 ± 6.4%. This was significantly ($p < 0.05$) more block than was obtained at pH 7.2 (29.1 ± 5.4% inhibition). At pH 8.9, MII toxin was ineffective. These results are consistent with a role for one or more protonated histidine residues in determining MII toxin potency but do not distinguish between histidine residues on the toxin and those on the receptor. However, within a model of the $\alpha 3\beta 2$ receptor extracellular domain (*9*), the region surrounding the ACh binding site where determinants of MII sensitivity have been identified (*10*) contains only one histidine residue (H186). Mutation of this histidine has been shown to have no effect on the sensitivity of the receptor to MII blockade (*10*). Thus, it is the protonated imidazolium form of at least one of the histidine residues on the MII toxin that is important for the toxin−receptor interaction.

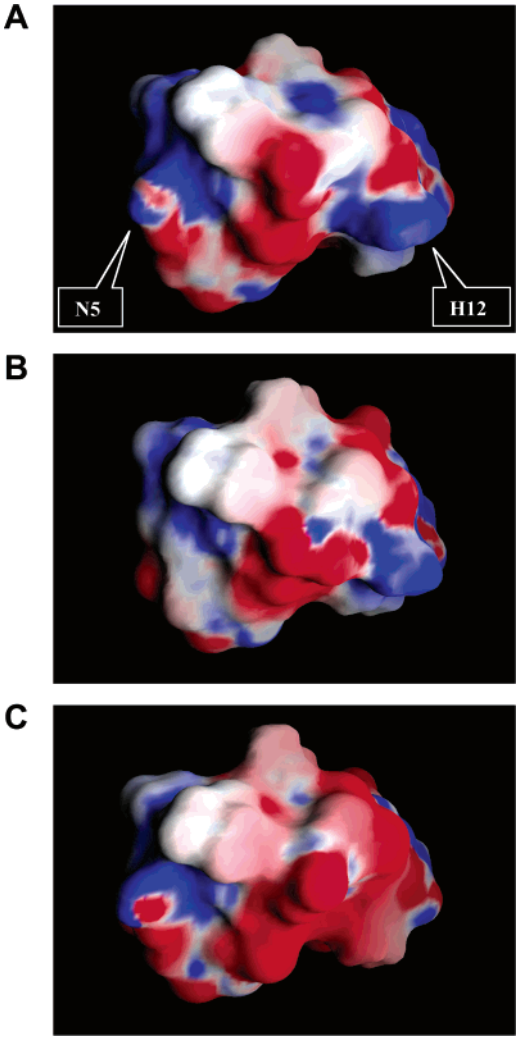

FIGURE 5: Molecular surfaces of wild-type and mutant MII toxins, colored by local electrostatic potential. (A) The electrostatic surface of the lowest energy NMR structure from Shon et al. (*14*) is shown. The N5 and H12 residue side chains are indicated. (B) The homology-modeled N5A mutant. (C) The homology-modeled H12A mutant. Images were generated using GRASP (*18*). The surface potential range is −3.0 (red) to +3.0 (blue).

In Figure 5A, we show the calculated electrostatic surface potential of the wild-type MII toxin. The small protrusion of N5 is indicated on the left. In the N5A mutant, both the positive and negative charge contributions are lost (Figure 5B). The large protrusion of H12 is indicated on the right side of the wild-type toxin. On the basis of the results of the pH dependence experiments, we show H12 in the charged form. Thus, this residue makes a strong positive contribution in this region. In the H12A mutant, both the large protrusion and the positive charge are lost (Figure 5C).

DISCUSSION

We have synthesized and screened a series of alanine-substituted mutants of α-conotoxin MII. Three of these mutants were dramatically less potent than the wild-type toxin. The N5A, P6A, and H12A mutations resulted in a >2700-fold, 700-fold, and ~2700-fold loss in potency, respectively (Table 1). This is striking, considering that mutation of adjacent residues (S4A, V7A, E11A, and S13A) had only modest effects. Circular dichroism analysis and molecular modeling suggested that the N5A, P6A, and H12A mutants were conformationally similar to wild-type MII toxin. For N5 and H12, these results support the view that the large loss in toxin potency is due to the loss of the asparagine or histidine side chains and not due to large alterations in toxin secondary structure. For P6, it may be the loss of the proline that is affecting toxin potency. However, the alanine substitution might also have an effect by altering the position of the N5 side chain.

We found MII antagonism of the α3β2 receptor to be sensitive to alterations in pH (Figure 4), consistent with a role for histidine side chains in the toxin−receptor interaction. The first pK_a for protonation of an imidazole nitrogen in histidine residues can vary, depending on the local environment. However, if we assume a pK_a of 6.5, then at pH 7.2 (our standard conditions), approximately 20% of the histidine side chains would be protonated. At this pH, 3 nM MII toxin blocked receptor function by 29%. At a pH of 5.5, approximately 90% of the histidine side chains would be protonated. Under these conditions, 3 nM MII toxin was more potent, blocking α3β2 receptors by 56%. At pH 8.9, with less than 1% of histidine residues protonated, 3 nM MII was inactive. These results indicate that one or more protonated histidines are critical participants in the interaction between MII toxin and the α3β2 receptor.

Previous mutagenesis of the α3β2 receptor (*10*) rules out a role for histidine residues on the receptor, suggesting that protonation of one or both of the histidines on the MII toxin itself is required for toxin potency. At present, we cannot be certain whether it is protonation of H9, H12, or both that is required. When displaying the electrostatic potential of the toxin surface, we have assigned a +1 charge to both H9 and H12 (Figure 5). The H9 side chain is partially buried within the toxin structure, and mutation of H9 has a relatively minor effect on toxin potency. In contrast, H12 forms a prominent protrusion on the toxin surface, and mutating H12 has a major effect on potency. Thus it is attractive to think that it is a charged H12 that is important in the toxin−receptor interaction. The other major determinants of toxin potency, N5 and P6, are located at the opposite end of the toxin. N5 provides a small protrusion with both positive and negative character. Between these two regions is a patch of pronounced negative charge that is provided by E11 and by the two disulfide bonds (C2−C8, C3−C16). The side chain of E11 is clearly not required for toxin potency (Figure 2 and Table 1). However, the region of negative charge provided by the cysteines, located between N5 and H12, may be part of the receptor interaction surface of the toxin.

We previously identified several residues (α3K185, α3I188, and β2T59) as determinants of MII sensitivity on the α3β2 receptor (*10*). In α subunits that form receptors that are less sensitive to MII blockade, I188 of α3 is replaced by lysine (α2) or arginine (α4). Similarly, T59 of β2 is replaced by lysine in β4. Our current results indicating that the N5 and H12 residues of MII toxin are critical determinants of toxin potency suggest that the role of α3I188 and β2T59 might not be through direct interaction with the MII toxin. Rather, it may be the presence of positively charged residues at either of these positions on the receptor that destabilizes the interaction between toxin and receptor through charge repulsion. If this were the case, then the positively charged protrusion of H12, and possibly N5, might be interacting with negatively charged residues on the receptor. These

residues would not necessarily be unique to the toxin-sensitive subunits. Examination of our previously published model of the α3β2 extracellular domain (*9*) suggests two residues on the β2 subunit as candidates to play such a role. Both of these residues are conserved in the β4 subunit. The side chain of glutamate 61 is 6.3 Å from β2T59, while aspartate 169 is 6.7 Å from α3I188. If a positively charged region of the MII toxin were interacting with either of these residues, insertion of a positive charge nearby would be likely to destabilize the interaction. The side chains of β2E61 and β2D169 are 17 Å apart, while the width of the MII toxin measured from N5 to H12 is 15 Å, suggesting that it would be possible for the MII toxin to interact with both of these residues.

While the MII toxin was initially thought to be selective for the α3β2 receptor, it has recently become clear that MII also antagonizes receptors containing the α6 subunit (*5*, *8*). This is not surprising given the high homology between the α3 and α6 subunits and, in particular, the conservation of both identified α subunit determinants of MII sensitivity (K185 and I188) in the α6 subunit (*19*). Two other "α3β2-selective" toxins, α-Ctx-PnIA and κ-bungarotoxin, have also been shown to antagonize α6-containing receptors (*9*). Recent evidence implicating α6-containing receptors in nicotine-mediated dopamine release (*20*) underscores a need for the development of probes capable of distinguishing among these closely related neuronal nAChRs.

We previously identified several residues on the α3β2 neuronal nAChR that determine sensitivity to α-Ctx-MII antagonism (*10*). We have now identified asparagine 5, proline 6, and histidine 12 on the α-Ctx-MII peptide as major determinants of toxin potency. Future experiments will involve examining the interaction between mutant toxins and mutant receptors. This approach will allow us to refine our understanding of the interaction between antagonists and the ligand-binding site of neuronal nicotinic receptors.

ACKNOWLEDGMENT

We thank Floyd Maddox, Ana Mederos, and Georgianna Guzman for excellent technical assistance.

REFERENCES

1. Karlin, A., and Akabas, M. H. (1995) Toward a structural basis for the function of nicotinic acetylcholine receptors and their cousins, *Neuron 15*, 1231−1244.
2. Corringer, P. J., Le Novere, N., and Changeux, J. P. (2000) Nicotinic receptors at the amino acid level, *Annu. Rev. Pharmacol. Toxicol. 40*, 431−458.
3. McIntosh, J. M., Santos, A. D., and Olivera, B. M. (1999) *Conus* peptides targeted to specific nicotinic acetylcholine receptor subtypes, *Annu. Rev. Biochem. 68*, 59−88.
4. Cartier, G. E., Yoshikami, D., Gray, W. R., Luo, S., Olivera, B. M., and McIntosh, J. M. (1996) A new α-conotoxin which targets α3β2 nicotinic acetylcholine receptors, *J. Biol. Chem. 271*, 7522−7528.
5. Gerzanich, V., Kuryatov, A., Anand, R., and Lindstrom, J. (1997) "Orphan" α6 nicotinic AChR subunit can form a functional heteromeric acetylcholine receptor, *Mol. Pharmacol. 51*, 320−327.
6. Luo, S., Nguyen, T. A., Cartier, G. E., Olivera, B. M., Yoshikami, D., and McIntosh, J. M. (1999) Single-residue alteration in α-conotoxin PnIA switches its nAChR subtype selectivity, *Biochemistry 38*, 14542−14548.
7. Hogg, R. C., Miranda, L. P., Craik, D. J., Lewis, R. J., Alewood, P. F., and Adams, D. J. (1999) Single amino acid substitutions in α-conotoxin PnIa shift selectivity for subtypes of the mammalian neuronal nicotinic acetylcholine receptor, *J. Biol. Chem. 274*, 36559−36564.
8. Kuryatov, A., Olale, F., Cooper, J., Choi, C., and Lindstrom, J. (2000) Human α6 AChR subtypes: subunit composition, assembly and pharmacological responses, *Neuropharmacology 39*, 2570−2590.
9. Everhart, D., Reiller, E., Mirzoian, A., McIntosh, J. M., Malhotra, A., and Luetje, C. W. (2003) Identification of residues that confer α-conotoxin PnIA sensitivity on the α3 subunit of neuronal nicotinic acetylcholine receptors, *J. Pharmacol. Exp. Ther. 306*, 664−670.
10. Harvey, S. C., McIntosh, J. M., Cartier, G. E., Maddox, F. N., and Luetje, C. W. (1997) Determinants of specificity for α-conotoxin MII on α3β2 neuronal nicotinic receptors, *Mol. Pharmacol. 51*, 336−342.
11. Harvey, S. C., and Luetje, C. W. (1996) Determinants of competitive antagonist sensitivity on neuronal nicotinic receptor β subunits, *J. Neurosci. 16*, 3798−3806.
12. Chen, Y. H., and Yang, J. T. (1971) A new approach to the calculation of secondary structures of globular proteins by optical rotatory dispersion and circular dichroism, *Biochem. Biophys. Res. Commun. 44*, 1285−1291.
13. Sali, A., and Blundell, T. L. (1993) Comparative protein modelling by satisfaction of spatial restraints, *J. Mol. Biol. 234*, 779−815.
14. Shon, K., Koerber, S. C., Rivier, J., Olivera, B. M., and McIntosh, J. M. (1997) Three-dimensional solution structure of α-conotoxin MII, an α3β2 neuronal nicotinic acetylcholine receptor-targeted ligand, *Biochemistry 36*, 15693−15700.
15. Laskowski, R. A., MacArthur, M. W., Moss, D. S., and Thornton, J. M. (1993) PROCHECK: a program to check the stereochemical quality of protein structures, *J. Appl. Crystallogr. 26*, 283−291.
16. Carson, M. (1997) Ribbons, *Methods Enzymol. 277*, 493−505.
17. Kleywegt, G. J. (1999) Experimental assessment of differences between related protein crystal structures, *Acta Crystallogr., D: Biol. Crystallogr. 55*, 1878−1884.
18. Nicholls, A., Sharp, K. A., and Honig, B. (1991) Protein Folding and Association: Insights From the Interfacial and Thermodynamic Properties of Hydrocarbons, *Proteins: Struct., Funct., Genet. 11*, 281−196.
19. Lamar, E., Miller, K., and Patrick, J. (1990) Amplification of genomic sequences identifies a new gene, alpha 6, in the nicotinic acetylcholine receptor gene family, *Soc. Neurosci. Abstr. 16*, 681.
20. Champtiaux, N., Han, Z. Y., Bessis, A., Rossi, F. M., Zoli, M., Marubio, L., McIntosh, J. M., and Changeux, J. P. (2002) Distribution and pharmacology of alpha 6-containing nicotinic acetylcholine receptors analyzed with mutant mice, *J. Neurosci. 22*, 1208−1217.

BI036180H